
The Spectrum of Fisher Information of Deep Networks Achieving Dynamical Isometry

Tomohiro Hayase
Fujitsu Laboratories,
Japan

Ryo Karakida
AIST,
Japan

Abstract

The Fisher information matrix (FIM) is fundamental for understanding the trainability of deep neural networks (DNN) since it describes the local metric of the parameter space. We investigate the spectral distribution of the FIM given a single input by focusing on fully-connected networks achieving dynamical isometry. Then, while dynamical isometry is known to keep specific backpropagated signals independent of the depth, we find that the parameter space’s local metric depends on the depth. In particular, we obtain an exact expression of the spectrum of the FIM given a single input and reveal that it concentrates around the depth point. Here, considering random initialization and the wide limit, we construct an algebraic methodology to examine the spectrum based on free probability theory, which is the algebraic wrapper of random matrix theory. As a byproduct, we provide the solvable spectral distribution in the two-hidden-layer case. Lastly, we empirically confirm that the spectrum of FIM with small batch-size has the same property as the single-input version. An experimental result shows that FIM’s dependence on the depth determines the appropriate size of the learning rate for convergence at the initial phase of the online training of DNNs.

1 Introduction

Deep neural networks (DNNs) have empirically succeeded in achieving high performances in various machine-learning tasks [1, 2]. Nevertheless, its theoretical understanding has been limited, and its success depends a lot on a heuristic search of settings such as architectures and hyper-parameters. To understand and improve the training of DNNs, researchers have developed some theories to investigate, for instance, exploding or vanishing gradient problems [3], the shape of the loss landscape [4, 5], the global convergence of training and the generalization [6].

The Fisher information matrix (FIM) is a fundamental quantity for such theoretical understandings. It describes a local metric of the loss surface concerning KL-divergence [4, 7, 8]. In particular, its eigenvalue spectrum describes the efficiency of optimization methods. For instance, the maximum eigenvalue determines an appropriate size of the learning rate of the first-order gradient method for convergence [5, 9]. Despite its importance, FIM’s spectrum in neural networks is not revealed enough from a theoretical perspective. It has been limited to random matrix theory for shallow networks [4] or mean-field theory for bounds of eigenvalues, which may be loose in general [8]. We need alternative approach applicable to deep networks.

When we analyze the spectrum of deep networks, we often face mathematical difficulties caused by non-linearity of activation and the network depth. Moreover, we face another essential problem on trainability, that is, naive settings (i.e., activation function and initialization) cause exploding or vanishing gradients at large depth. To avoid the exploding/vanishing gradient problems, it is necessary that the model satisfies *dynamical isometry* [10, 11]. We say that a network achieves dynamical isometry if its input-output Jacobian’s all singular values are one. The previous works [11–13] found

that DNNs achieve approximately dynamical isometry through random orthogonal weights, but do not through random Gaussian weights.

The present work aims to investigate the asymptotic spectrum of the FIM of multi-layer perceptrons satisfying the dynamical isometry. To handle the mathematical difficulties to treat the spectrum, we focus on a pointwise FIM given a single input and use free probability theory (FPT). The FPT, which is invented by Voiculescu for understanding von Neuman algebras [14], provides an algebraic wrapper of random matrix theory [15]. In particular, FPT provides tools to compute the asymptotic eigenvalue of a random matrix polynomial from that of each component matrix constituting the polynomial. Since DNN’s FIM is a random matrix polynomial of the Jacobian, FPT provides tools for understanding FIM’s spectral distribution. We use these tools to obtain the propagation of spectral distributions through layers.

Our findings are as follows. Firstly, consider DNNs achieving dynamical isometry. We find that the FIM’s asymptotic spectrum depends on the At large depth, and eigenvalues of the pointwise FIM concentrate around the value of depth. This phenomenon is in contrast to the spectrum of input-output Jacobian, which is independent of the depth. It suggests that the local geometry of the parameter space primarily depends on the depth and the first-order optimization also suffers from it. Secondly, we find a solvable case of the spectrum in the deep case. We explicitly show the asymptotic spectrum of the pointwise FIM with two hidden layers (total three layers) under some situation. This solvable model helps understand the effect of dynamical isometry on the spectrum and the connection to a universal law of random matrices in FPT. Thirdly, we empirically confirm that the spectrum of FIM with small batch-size has the same property as the single-input version. Lastly, an experimental result shows that FIM’s dependence on the depth determines an appropriate size of the learning rate for convergence at the initial phase of the online training of DNNs.

Our analysis is the first step of theoretical understanding of the FIM. We expect that the spectrum of other FIMs in more various settings will be obtained by extending our framework.

1.1 Related Works

Several works have analyzed the eigenvalues of FIM in limited cases. Pennington-Worah [4] analyzed the spectrum of FIM via random matrix theory but limited to shallow networks and random Gaussian weight matrices. Karakida et al. [5, 8] obtained some bounds for FIM’s eigenvalues in deep networks, but their bounds are loose in general and also limited to Gaussian weights. [10] treats eigenvalues of the loss’s Hessian, but the work is restricted to DNNs with linear activation. In contrast, we investigate the FIM spectrum of deep non-linear networks on random orthogonal weights, which satisfy the dynamical isometry.

Additionally, we remark that [6] uses a version of the dual FIM Θ with Gaussian initialization as a kernel matrix and call it the neural tangent kernel (NTK). The eigenvalues of FIM also determine the convergence properties of gradient descent in wide neural networks through the NTK.

2 Preliminaries

2.1 Settings

Network Architecture We assume random weight matrices as is usual in the studies of FIM [4, 5] and dynamical isometry [10, 11]. Fix $L \in \mathbb{N}$. We consider a L -layer feed-forward neural network f_θ with weight matrices $\theta = (W_1, W_2, \dots, W_L) \in M_M(\mathbb{R})^L$ and pointwise activation functions $\varphi^1, \dots, \varphi^{L-1} \in C(\mathbb{R})$. Besides, we assume that φ^ℓ is differentiable except for finite points. Firstly, pick a single input $x \in \mathbb{R}^M$. Set $x^0 = x$. For $\ell = 1, \dots, L$, set

$$h^\ell = W_\ell x^{\ell-1} + b^\ell, \quad x^\ell = \varphi^\ell(h^\ell). \quad (1)$$

We omit the bias parameters b^ℓ in (1) to simplify the analysis. Write

$$D_\ell = \frac{\partial x^\ell}{\partial h^\ell}, \quad \delta_{L \rightarrow \ell} = \frac{\partial h^L}{\partial h^\ell}. \quad (2)$$

Fisher Information Matrix We focus on the *Fisher information matrix* (FIM) for supervised learning with a mean squared error (MSE) loss [4, 8, 16]. Let us summarize its definition and

basic properties. Given $x \in \mathbb{R}^M$ and θ , we consider a Gaussian probability model $p_\theta(y|x) = \exp(-\mathcal{L}(f_\theta(x) - y)) / \sqrt{2\pi}$ ($y \in \mathbb{R}^M$). We define the MSE loss by $\mathcal{L}(u) = \|u\|^2/2$ ($u \in \mathbb{R}^M$), where $\|\cdot\|$ is the Euclidean norm. In addition, consider a probability distribution $p(x)$ and a joint distribution $p_\theta(x, y) = p_\theta(y|x)p(x)$. Then, the FIM $\mathcal{I}(\theta) \in M_{LM^2}(\mathbb{R})$ of p_θ is defined by $\mathcal{I}(\theta) = \int [\nabla_\theta \log p_\theta(x, y)]^\top \nabla_\theta \log p_\theta(x, y) p_\theta(x, y) dx dy$. Now, we denote by $\mathcal{I}(\theta|x)$ the conditional (or pointwise) FIM given a single input x ; $\mathcal{I}(\theta|x) = \int [\nabla_\theta \log p_\theta(y|x)]^\top \nabla_\theta \log p_\theta(y|x) p_\theta(y|x) dy$. Since we consider the Gaussian $p_\theta(y|x)$, we have

$$\mathcal{I}(\theta|x) = \frac{\partial f_\theta(x)}{\partial \theta}^\top \frac{\partial f_\theta(x)}{\partial \theta}. \quad (3)$$

Since the distribution $p(x)$ of the input does not depend on θ , the FIM is given by

$$\mathcal{I}(\theta) = \int \mathcal{I}(\theta|x) p(x) dx = \int \frac{\partial f_\theta(x)}{\partial \theta}^\top \frac{\partial f_\theta(x)}{\partial \theta} p(x) dx. \quad (4)$$

We regard $p(x)$ as an empirical distribution of input samples [4, 8, 17]. As is known in information geometry [7], the FIM works as a degenerate metric on the parameter space: the Kullback-Leibler divergence between the statistical model and itself perturbed by $d\theta$ is given by $D_{\text{KL}}(p_\theta || p_{\theta+d\theta}) = d\theta^\top \mathcal{I}(\theta) d\theta$. More intuitive understanding is that we can write the Hessian of the loss as $\frac{\partial^2}{\partial \theta^2} \mathbb{E}_{x,y}[\mathcal{L}(f_\theta(x) - y)] = \mathcal{I}(\theta) + \mathbb{E}_{x,y}[(f_\theta(x) - y)^\top \frac{\partial^2}{\partial \theta^2} f_\theta(x)]$. Hence the FIM also characterizes the local geometry of the loss surface around a global minimum with a zero training error.

Dual Fisher Information Matrix Now, in order to ignore $\mathcal{I}(\theta|x)$'s trivial eigenvalue zero, we introduce the *dual conditional (or pointwise) FIM* with a normalization given by

$$H_L(x, \theta) = \frac{1}{M} \frac{\partial f_\theta(x)}{\partial \theta} \frac{\partial f_\theta(x)}{\partial \theta}^\top. \quad (5)$$

If there is no confusion, we omit the arguments and simply write it H_L . Except for trivial zero eigenvalues, $\mathcal{I}(\theta|x)/M$ and $H_L(x, \theta)$ share eigenvalues. We use the normalization factor $1/M$ since the loss $\mathcal{L}(y)$ is $O(M)$ as $M \rightarrow \infty$ when the output y has the constant order second moments.

2.2 Notations

Spectral Distribution Recall that the spectral distribution μ of a linear operator A is a probability distribution μ on \mathbb{R} such that $\text{tr}(A^m) = \int t^m \mu(dt)$ for any $m \in \mathbb{N}$, where tr is the normalized trace. If A is an $M \times M$ symmetric matrix with $M \in \mathbb{N}$, its spectral distribution is given by $M^{-1} \sum_{k=1}^M \delta_{\lambda_k}$, where λ_k ($k = 1, \dots, M$) are eigenvalues of A , and δ_λ is the discrete probability distribution whose support is $\{\lambda\} \subset \mathbb{R}$.

S-transform Given probability distribution ν , set $G_\nu(z) = \int (z - t)^{-1} \nu(dt)$ and $h_\nu(z) = zG_\nu(z) - 1$. Then the S-transform [18] of ν is defined as

$$S_\nu(z) = \frac{1+z}{z} \frac{1}{h_\nu^{-1}(z)}. \quad (6)$$

For example, given discrete distribution $\nu = \alpha \delta_0 + (1 - \alpha) \delta_\gamma$ with $0 \leq \alpha \leq 1$ and $\gamma > 0$, we have $S_\nu(z) = \gamma^{-1}(z + \alpha)^{-1}(z + 1)$. If two operators A and B are free and each spectral distribution is given by μ and ν respectively, then the spectral distribution of AB is given by the free multiplicative convolution, denoted by $\mu \boxtimes \nu$ [18]. Moreover, it holds that

$$S_{\mu \boxtimes \nu}(z) = S_\mu(z) S_\nu(z). \quad (7)$$

3 Propagation of Spectral Distributions

3.1 Recursive Equations

We use several assumptions in mean-field theory of neural networks [5, 11, 19]. Firstly, we assume that W_ℓ/σ_ℓ are independent and uniformly distributed on $M \times M$ orthogonal matrices, where

$\sigma_1, \dots, \sigma_L > 0$ are constant. Secondly, set $\hat{q}_\ell = \|x_\ell\|^2/M$. Assume that \hat{q}_0 converges to $q_0 > 0$. With an appropriate choice of activation function, the empirical distribution of each hidden unit x_ℓ converges to the centered normal distribution [11]. Set $q_\ell = \lim_{M \rightarrow \infty} \hat{q}_\ell$. Lastly, we assume the following asymptotic freeness. (We refer readers to [20, 21] and the supplemental material C for more information on asymptotic freeness.)

Assumption 3.1. We assume that $(D_\ell)_{\ell=1}^{L-1}$ is asymptotically free from $(W_\ell, W_\ell^\top)_{\ell=1}^L$ as $M \rightarrow \infty$ almost surely.

Note that Assumption 3.1 is weaker than the assumption of the forward-backward independence often used in mean-field theory [5, 11, 19]. Several works prove or treat the asymptotic freeness with Gaussian initialization [22–24], and we expect that it will also hold with orthogonal initialization.

Now we have prepared to discuss a propagation of spectral distributions. It holds that $H_L = \sum_{\ell=1}^L \hat{q}_{\ell-1} \delta_{L \rightarrow \ell} \delta_{L \rightarrow \ell}^\top$. Since $\delta_{L \rightarrow \ell} = W_L D_{L-1} \delta_{L-1 \rightarrow \ell}$ ($\ell < L$), it holds that

$$H_{\ell+1} = \hat{q}_\ell I + W_{\ell+1} D_\ell H_\ell D_\ell^\top W_{\ell+1}^\top, \quad (8)$$

where I is the identity matrix. Let μ_ℓ (resp. ν_ℓ) is the limit spectral distribution as $M \rightarrow \infty$ of H_ℓ (resp. D_ℓ^2). Note that $\mu_1 = \delta_{q_0}$. By Assumption 3.1, we have the following propagation equation of spectral distributions. For $\ell = 1, \dots, L-1$, we have

$$\mu_{\ell+1} = (q_\ell + \sigma_{\ell+1}^2 \cdot)_* (\nu_\ell \boxtimes \mu_\ell), \quad (9)$$

where given distribution μ , the distribution $(b + a \cdot)_* \mu$ is the pushforward of μ with the map $x \mapsto b + ax$.

3.2 An Example: The Two-Hidden-Layer Case

To show a nontrivial example, we examine the solvable asymptotic spectrum of the pointwise FIM in the case of a two-hidden-layer network (i.e. $L = 3$). Assume that

$$\nu_\ell = (1 - \alpha_\ell) \delta_0 + \alpha_\ell \delta_{\gamma_\ell}, \quad (10)$$

where $0 < \alpha_\ell < 1$ and $\gamma_\ell > 0$. We get the distribution (10) if we choose activation as the shifted-ReLU ($\varphi(x) = ax$ if $x > b$ otherwise ab with $a, b > 0$) or the hard tanh given by

$$\varphi_{s,g}(x) = \begin{cases} gx, & \text{if } sg|x| < 1, \\ g \cdot \text{sgn}(x), & \text{otherwise,} \end{cases} \quad (11)$$

where $s, g > 0$. These activation function appears in [11] for dynamical isometry. Then we have the following explicit representation of the H_3 's asymptotic spectral distribution μ_3 .

Theorem 3.2. We have $\mu_3(dx) = \mu_{\text{atoms}}(dx) + \rho(x)dx$, where

$$\mu_{\text{atoms}} = (1 - \alpha_2) \delta_{\lambda_{\min}} + (\alpha_2 - \alpha_1)^+ \delta_{\lambda_{\text{mid}}} + (\alpha_1 + \alpha_2 - 1)^+ \delta_{\lambda_{\max}}(dx), \quad (12)$$

$$\rho(x) = \frac{\sqrt{(\lambda_+ - x)(x - \lambda_-)}}{2\pi(x - \lambda_{\text{mid}})(\lambda_{\max} - x)} \mathbf{1}_{[\lambda_-, \lambda_+]}(x), \quad (13)$$

with the following notations: $a^+ = \max(a, 0)$ for $a \in \mathbb{R}$, $\mathbf{1}_X$ is the indicator function for $X \subset \mathbb{R}$,

$$\lambda_{\min} = q_2, \quad (14)$$

$$\lambda_{\text{mid}} = q_2 + \sigma_3^2 \gamma_2 q_1, \quad (15)$$

$$\lambda_{\pm} = q_2 + \sigma_3^2 \gamma_2 \left(q_1 + \sigma_2^2 \gamma_1 q_0 \left(\sqrt{\alpha_1(1 - \alpha_2)} \pm \sqrt{\alpha_2(1 - \alpha_1)} \right)^2 \right), \text{ and} \quad (16)$$

$$\lambda_{\max} = q_2 + \sigma_3^2 \gamma_2 (q_1 + \sigma_2^2 \gamma_1 q_0). \quad (17)$$

Proof. The proof is based on (7) and (9), and is postponed to the supplemental material A. \square

Fig. 1 shows the agreement of the predicted distribution μ_3 by Theorem 3.2 and the empirical spectral distribution of H_3 . We observed in Fig. 1 (left) that most of the eigenvalues were concentrated at the value of depth when a DNN achieved dynamic isometry, but there were other peaks. Theorem 3.2

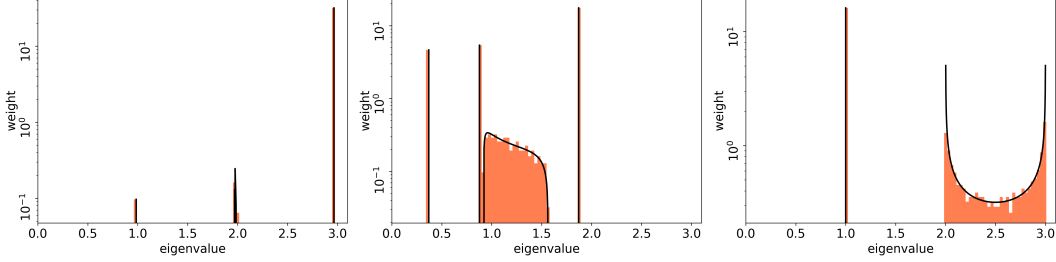


Figure 1: Normalized histograms of eigenvalues of H_3 (orange) and predicted μ_3 by Theorem 3.2 (black lines). The y-axis in each figure is logarithmic. We set $M = 1000$, $\hat{q}_0 = \sigma_\ell = 1$, the width of bins 0.31, and used the following setting. (Left): We used the hard tanh activation (11) with $s = 0.125$ and $g = 1.0013$ to achieve dynamical isometry. (Center): We used the hard tanh with $s = g = 1$. (Right): We constructed H_L based on (8) by replacing each Jacobian D_ℓ with an independent matrix whose spectral distribution is $(1/2)\delta_0 + (1/2)\delta_1$.

reveals that the weight of the minimum eigenvalue depends on how much the last activation's derivation vanishes. Later, we show in Theorem 4.6 that the eigenvalues concentrate on the value of depth at the large depth. Next, we observed in Fig. 1 (center) that the eigenvalues varied when a DNN was out of dynamical isometry. Although Fig. 1 (right) is also out of dynamical isometry, the spectrum obeys the arcsin law known in FPT [20] and is interesting its own right. Once the hyperparameters are standardized and each D_ℓ is a projection, the spectrum is attributed to the product of free two projections well examined in FPT.

4 Analysis through Dynamical Isometry

4.1 Review on Dynamical isometry

Let us review on how to achieve the dynamical isometry. For the sake of the prospect of the theory, let J be the Jacobian of the network with ignoring the last layer $h^L \mapsto x^L = W_L h^L$. We say that the network achieves dynamical isometry if all eigenvalues of JJ^T are one. Consider the limit spectral distribution ν_ℓ of D_ℓ^2 given by (10). At the deep limit, we consider the situation such that forward and backward signal propagation are stable. Hence we adopt the following assumption,

Assumption 4.1. For each $L \in \mathbb{N}$, sequences $q_\ell, \alpha_\ell, \gamma_\ell$ and $\sigma_{\ell+1}$ ($\ell = 0, 1, \dots, L-1$) are constant for every ℓ , but depend on L . In addition, each constant converges to a finite value as $L \rightarrow \infty$.

Now the limit spectral distribution of $J^T J$ as $M \rightarrow \infty$ is given by $[(\sigma_{L-1}^2 \cdot)_* \nu_{L-1}]^{\boxtimes(L-1)}$. By (7),

$$S_{[(\sigma_{L-1}^2 \cdot)_* \nu_{L-1}]^{\boxtimes(L-1)}}(z) = \frac{1}{(\sigma_{L-1}^2 \gamma_{L-1})^{L-1}} \left(1 + \frac{1 - \alpha_{L-1}}{z + \alpha_{L-1}}\right)^{L-1}. \quad (18)$$

In order to achieve dynamical isometry, we need that $[(\sigma_{L-1}^2 \cdot)_* \nu_{L-1}]^{\boxtimes(L-1)}$ converges to a compactly supported distribution as $L \rightarrow \infty$, and $S_{JJ^T}(z)$ converges to a non-zero function of z . Since the right hand side is approximated by $\exp(L(1 - \alpha_L)(z + \alpha_L)^{-1} - L \log \sigma_L^2 \gamma_L)$ as $L \rightarrow \infty$, we need $\log \sigma_L^2 \gamma_L = O(L^{-1})$ and $1 - \alpha_L = O(L^{-1})$ as $L \rightarrow \infty$. To consider approximate dynamical isometry, which are treated in [11], we consider the following weaker condition.

Assumption 4.2. Each limit $\lim_{L \rightarrow \infty} L(1 - \alpha_L)$ and $\varepsilon_2 = -\lim_{L \rightarrow \infty} L \log \sigma_L^2 \gamma_L$ exists and $|\varepsilon_1|, |\varepsilon_2| < 1$.

To achieve exact dynamical isometry, we need the limit S -transform is 1, in particular $\varepsilon_1 = \varepsilon_2 = 0$.

4.2 Statistics of dual conditional FIM

Firstly, we show that the mean of spectrum is $O(L)$ as $L \rightarrow \infty$.

Proposition 4.3. Under Assumption 4.1 and 4.2, it holds that

$$\lim_{L \rightarrow \infty} L^{-1} m_1(\mu_L) = q(\varepsilon_1 + \varepsilon_2)^{-1} [1 - \exp(-\varepsilon_1 - \varepsilon_2)], \quad (19)$$

where $q = \lim_{L \rightarrow \infty} q_L$. In particular, the limit has the expansion $q(1 + (\varepsilon_1 + \varepsilon_2)/2) + O((\varepsilon_1 + \varepsilon_2)^2)$ as $\varepsilon_1, \varepsilon_2 \rightarrow 0$.

Proof. We have $m_1(\mu_{L+1}) = \sum_{\ell=0}^L q_\ell (\sigma_{\ell+1}^2 \alpha_\ell \gamma_\ell)^\ell = q_L \sum_{\ell=0}^L (\sigma_{L+1}^2 \alpha_L \gamma_L)^\ell$ by Assumption 4.1. Set $x_L = L(1 - \sigma_{L+1}^2 \alpha_L \gamma_L)$. We have $\lim_{L \rightarrow \infty} x_L = \varepsilon_1 + \varepsilon_2$. Then $L^{-1} \sum_{\ell=0}^L (\sigma_{L+1}^2 \alpha_L \gamma_L)^\ell = x_L^{-1} [1 - (1 - x_L/L)^L] \rightarrow (\varepsilon_1 + \varepsilon_2)^{-1} (1 - \exp(-\varepsilon_1 - \varepsilon_2))$. Then the assertion has been proven. \square

Secondly, we examine the maximal eigenvalue of H_L . For a compactly supported probability measure ν on \mathbb{R}_+ , we denote by $\|\nu\|_\infty$ the maximum of the support of ν . We prove that $\|\nu_L\|_\infty$ is an atom of ν_L . Recall that $x \in \mathbb{R}$ is an atom of a probability distribution ν if and only if $\nu(\{x\}) > 0$.

Let us review on the following proposition known in free probability theory.

Proposition 4.4 ([25]). *Let μ and ν be compactly supported probability distributions on \mathbb{R} . Then $\mu \boxtimes \nu$ has an atom at $c \in \mathbb{R}$ if and only if the following three conditions hold: (i) $a \in \mathbb{R}$ (resp. $b \in \mathbb{R}$) is an atom of μ (resp. ν), (ii) $c = ab$, and (iii) $\mu(\{a\}) + \nu(\{b\}) - 1 > 0$. Furthermore, if c is an atom then $\mu \boxtimes \nu(\{c\}) = \mu(\{a\}) + \nu(\{b\}) - 1$.*

Then we have the following recurrence equation of the maximum eigenvalue.

Lemma 4.5. *Fix $L \in \mathbb{N}$. Let $\beta_1 = 1$ and $\beta_\ell = 1 - \sum_{k=1}^{\ell-1} (1 - \alpha_k)$ for $\ell \geq 2$. Assume that $\beta_L > 0$. Then for any $\ell \leq L$, the value $\|\mu_\ell\|_\infty$ is an atom of μ_ℓ with weight β_ℓ . Furthermore, we have $\|\mu_\ell\|_\infty = q_{\ell-1} + \sigma_\ell^2 \gamma_{\ell-1} \|\mu_{\ell-1}\|_\infty$ for $\ell \neq 1$.*

Proof. Let us define $\lambda_\ell \in \mathbb{R}$ recursively by $\lambda_\ell = q_{\ell-1} + \sigma_\ell^2 \gamma_{\ell-1} \lambda_{\ell-1}$ ($\ell \geq 2$) and $\lambda_1 = q_0$. Firstly we prove that λ_ℓ is an atom with weight β_ℓ of μ_ℓ for $\ell \leq L$. In the case $\ell = 1$, we have $\mu_1 = \delta_1 = \delta_{\lambda_1}$. Fix $\ell > 1$ and assume that $\lambda_{\ell-1}$ is an atom of $\mu_{\ell-1}$ with weight $\beta_{\ell-1}$. Now $\beta_{\ell-1} + \alpha_{\ell-1} - 1 = \beta_\ell \geq \beta_L > 0$. Hence by Proposition 4.4, $\nu_{\ell-1} \boxtimes \mu_{\ell-1}$ has an atom $\gamma_{\ell-1} \lambda_{\ell-1}$ with weight β_ℓ . Therefore μ_ℓ has the atom λ_ℓ with weight β_ℓ . The claim follows from the induction on ℓ . To complete the proof, we only need to show that $\lambda_\ell = \|\mu_\ell\|_\infty$. Clearly $\lambda_\ell \leq \|\mu_\ell\|_\infty$. Note that $\|\mu \boxtimes \nu\|_\infty \leq \|\mu\|_\infty \|\nu\|_\infty$. Then $\|\mu_\ell\|_\infty \leq q_{\ell-1} + \sigma_\ell^2 \gamma_{\ell-1} \|\mu_{\ell-1}\|_\infty$. Thus it holds that $\|\mu_\ell\|_\infty \leq \lambda_\ell$ since $\|\mu_1\|_\infty = q_0 = \lambda_1$. Hence the claim follows. \square

Now we have prepared to prove the desired theorem.

Theorem 4.6. *Consider Assumption 4.1 and 4.2. Then for sufficiently larger L , it holds that $\|\mu_L\|_\infty$ is an atom of μ_L with weight $1 - (L-1)(1 - \alpha_{L-1})$, and*

$$\lim_{L \rightarrow \infty} L^{-1} \|\mu_L\|_\infty = q \varepsilon_2^{-1} [1 - \exp(-\varepsilon_2)]. \quad (20)$$

In particular, the limit has the expansion $q(1 + \varepsilon_2/2) + O(\varepsilon_2^2)$ as the further limit $\varepsilon_2 \rightarrow 0$.

Proof. Since $\varepsilon_1 < 1$, we have $1 - \alpha_{L-1} < (L-1)^{-1}$ for sufficiently large L . Then $\beta_L = 1 - (L-1)(1 - \alpha_{L-1}) > 0$. Hence by Lemma 4.5, for any $\ell \leq L$, it holds that $\|\mu_\ell\|_\infty$ is an atom of μ_ℓ and $\|\mu_L\|_\infty = q_L \sum_{\ell=0}^{L-1} (\sigma_L^2 \gamma_{L-1})^\ell$. Then by the same discussion as Proposition 4.3, the assertion follows. \square

Theorem 4.6 shows that the maximum eigenvalue of the pointwise FIM H_L is $O(L)$ as $L \rightarrow \infty$. Furthermore, we emphasize that the weight $1 - (L-1)(1 - \alpha_{L-1}) \sim 1 - \varepsilon_1$ of the maximal eigenvalue $\|\mu_L\|_\infty$ is close to 1. Therefore, eigenvalues of the dual pointwise FIM H_L concentrates around $qL(1 + \varepsilon_2/2)$, and the dual FIM approximates the scaled identity operator. Clearly the same property holds for non-zero eigenvalues of the pointwise FIM $\mathcal{I}(\theta|x)$.

4.3 Expected versus Pointwise Fisher Information

Fix $N \in \mathbb{N}$ and consider input vectors $x(1), \dots, x(N) \in \mathbb{R}^M$. Set $x^0(n) = x(n)$. Since $\mathcal{I}(\theta) = N^{-1} \sum_{n=1}^N \mathcal{I}(\theta|x(n))$, the FIM $\mathcal{I}(\theta)$ shares non-zero eigenvalues with the dual $\Theta \in M_N(\mathbb{R}) \otimes M_M(\mathbb{R})$ given by

$$\Theta(m, n) = \frac{1}{N} \sum_{n=1}^N \frac{\partial f_\theta(x(m))}{\partial \theta} \frac{\partial f_\theta(x(n))}{\partial \theta}^\top, \quad m, n = 1, \dots, N. \quad (21)$$

For $\ell = 1, \dots, L$, set recursively $h^\ell(n) = W_\ell x^{\ell-1}(n)$, $x^\ell(n) = \varphi^\ell(h^\ell(n))$, and define $\delta_{L \rightarrow \ell}(n)$ in the same way. Then $\Theta(m, n) = MN^{-1} \sum_{\ell=1}^L \Sigma_\ell(m, n) \delta_{L \rightarrow \ell}(m) \delta_{L \rightarrow \ell}(n)^\top$, where $\Sigma_\ell(m, n) = M^{-1} \sum_{i=1}^M x_{\ell,i}(m) x_{\ell,i}(n)$, and we have the following block-matrix representation:

$$\Theta = \frac{M}{N} \begin{bmatrix} H_L(x(1)) & * & \dots & * \\ * & H_L(x(2)) & \dots & * \\ \vdots & \dots & \ddots & \vdots \\ * & * & \dots & H_L(x(N)) \end{bmatrix}. \quad (22)$$

Hence for the N -sample, considering the collection of eigenvalues of the dual pointwise FIMs $(H_L(x(n)))_{n=1}^N$ is equivalent to considering block-diagonal approximation of the (scaled) dual FIM $MN^{-1}\Theta$. Even if it is not clear yet that the block-diagonal approximation behaves well, the mean of eigenvalues of full matrix is exactly determined by the diagonal part as the following assertion.

Corollary 4.7. *Denote by $m_{L,N}$ the wide limit $M \rightarrow \infty$ of the mean of eigenvalues of Θ/M . Then under the limit $L, N \rightarrow \infty$ with $L/N \rightarrow \alpha < \infty$, it holds that*

$$m_{L,N} \rightarrow \alpha q(\varepsilon_1 + \varepsilon_2)^{-1} [1 - \exp(-\varepsilon_1 - \varepsilon_2)]. \quad (23)$$

Proof. Fix L, N . The mean of eigenvalues of Θ/M is equal to $\text{tr}(\Theta/M)$ and $\text{tr}(\Theta/M) = \sum_{n=1}^N \text{tr}(H_L(x(n)))/N^2 \rightarrow m_1(\mu_L)/N$. By Proposition 4.3, the assertion follows. \square

Corollary 4.7 implies that the mean eigenvalue of Θ/M is close to qLN^{-1} when L and N are of the same magnitude. In the next section, we empirically examine the block-diagonal approximation.

5 Empirical Analysis

5.1 Expected vs Pointwise FIM

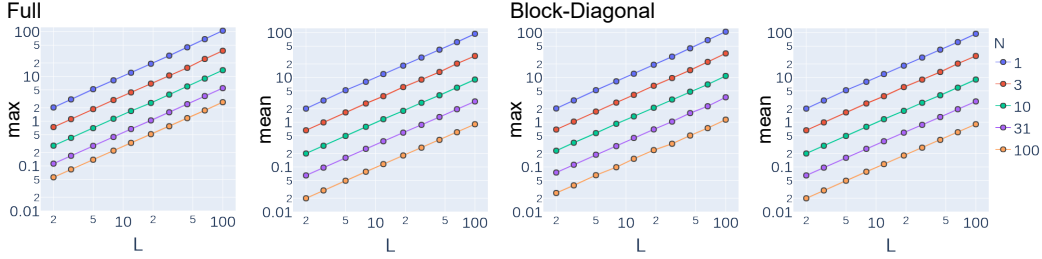


Figure 2: Eigenvalues of Θ/M (full matrix) and the collection of eigenvalues of $(H_L(x(n))/N)_{n=1}^N$ (one block); We show maximum and mean in each case. We set $M = 100$ and each axis logarithmic.

In order to investigate the difference between the FIM and the pointwise FIM for multi-inputs, we numerically computed eigenvalues of their dual matrices with $\hat{q}_0 = 1$. Fig. 2 shows the statistics of their eigenvalues of Θ/M (Full) and $(H_L(x(n))/N)_{n=1}^N$ (Block-Diag) with $L = N = 10$. We observed that the maximum and the mean eigenvalue of each matrix are $O(L/N)$, except for the maximum eigenvalue of Θ/M with large N .

Fig. 3 shows an example of eigenvalues of Θ/M (Full) and $(H_L(x(n))/N)_{n=1}^N$ (Block-Diag) concentrated around L/N for a small N . For the pointwise FIM, we observed theoretical predictions Proposition 4.3 and Theorem 4.6 agree well with experimental results.

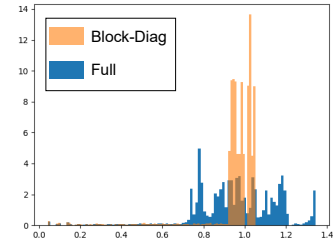


Figure 3: Histograms of eigenvalues.

5.2 Training Dynamics

To investigate the effect of the FIM’s spectrum on training, we see how well it correlates with the training dynamics. Consider the online gradient descent method: $\theta_{t+1} = \theta_t - \eta \nabla_{\theta} [M^{-1} \mathcal{L}(f_{\theta_t}(x(t)) - y(t))]$. Under the first order Taylor approximation of f_{θ} around the initial parameter θ_0 , we have the following approximation: $\theta_{t+1} \sim (I - \eta H_L(x(t), \theta_0)) \theta_t + M^{-1} f_{\theta_0}(x)^\top (y - f_{\theta_0}(x) + \nabla_{\theta} f_{\theta_0}(x(t))^\top \theta_0)$. Hence at the initial phase of the training, the condition $\|I - \eta H_L\| < 1$ is necessary to avoid the explosion of parameters. In particular, $\eta < 2/\lambda_{\max}(H_L)$. By Theorem 4.6, we expect that the boundary $2/\lambda_{\max}(H_L)$ will be close to $2/(qL)$.

To confirm the boundary, we exhaustively searched test loss, and test accuracy, while changing L and η with normalizing inputs with $\hat{q}_0 = 1$. In Fig. 4, we observed the theoretical prediction $\eta = 2/L$ coincided well with the boundary of the collapse of the accuracy obtained in experiments. We observed that the test loss slightly violates the boundary at large L (i.e., $\eta > 2/L$ and the test loss was not large). However, in this region, we found that the spectral distribution of H_L during training was far different from that in the initial state. (See the supplemental material B for the detail.) Thus, although the parameters do not explode, we have a qualitative change of the optimization in the seeping region. In this sense, the theoretical boundary explains well the state of training.

We applied the online gradient descent for 500 step. We trained the network on a benchmark dataset Fashion-MNIST [26], which contains 60000 samples of 28^2 dimensional vectors and 10 class labels. We normalized each input so that $\hat{q}_0 = 1$ and converted class labels to an orthonormal system in \mathbb{R}^M . In whole experiments, we commonly use the hard-tanh activation with $s = 0.125$ and $g = 1.0013$ to archive dynamical isometry. After training, we computed the MSE loss \mathcal{L}/M and accuracy on the dataset of 10000 samples separated from the dataset for training.

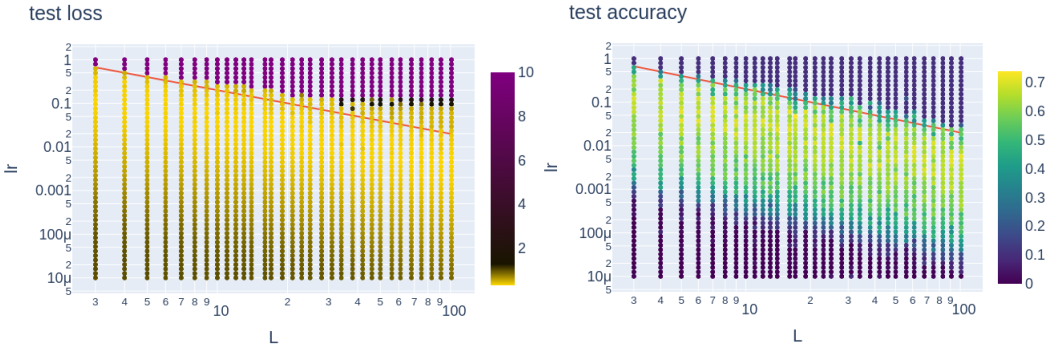


Figure 4: Heatmaps of loss (left) and accuracy (right) for different L (x-axis) and η (y-axis) under online training. The line in each figure is $\eta = 2/L$. Each axis is logarithmic.

6 Conclusion

Our study provides a springboard for a new way of examining Fisher information of neural networks with a powerful methodology provided by free probability theory. In particular, we have shown that eigenvalues of the dual pointwise FIM are concentrated on the maximum when a DNN achieves dynamical isometry approximately. Furthermore, we have solved a propagation equation and shown the exact form of the spectrum distribution in the depth three.

The evidence of the study suggests intimates that the empirical Fisher information matrix is of order L/N . This observation is consistent with a depth-dependent learning rate, which is empirically observed in [19] and required for the convergence of training in deep linear networks [27].

We are aware that our spectral analysis of the FIM may have limitations. A limitation is that our analysis is based on the asymptotic freeness of Jacobi matrices (Assumption 3.1). We expect that the works [22–24], which prove or treat the asymptotic freeness with Gaussian initialization, will help us to prove it with the orthogonal initialization. Another limitation is that the batch size is limited to be small in our theory. Future analysis of block random matrices via free probability theory will investigate the spectrum of the full Fisher information matrix.

Acknowledgments and Disclosure of Funding

The authors gratefully acknowledge valuable and profound comments of Roland Speicher, in particular about free probability theory. The authors would like to thank Hiroaki Yoshida and Noriyoshi Sakuma for constructive discussion. This research was supported by JST ACT-X JPMJAX190N.

Broader Impact

We believe that this section is not applicable to this paper.

References

- [1] Yann LeCun, Yoshua Bengio, and Geoffrey Hinton. Deep learning. *Nature*, 521(7553):436–444, 2015. ISSN 1476-4687. doi: 10.1038/nature14539. URL <https://doi.org/10.1038/nature14539>.
- [2] Ian Goodfellow, Yoshua Bengio, and Aaron Courville. *Deep Learning*. MIT Press, 2016.
- [3] Samuel S Schoenholz, Justin Gilmer, Surya Ganguli, and Jascha Sohl-Dickstein. Deep information propagation. *ICLR 2017*, *arXiv:1611.01232*, 2017.
- [4] Jeffrey Pennington and Pratik Worah. The spectrum of the Fisher information matrix of a single-hidden-layer neural network. In *Proceedings of Advances in Neural Information Processing Systems (NeurIPS)*, pages 5410–5419, 2018.
- [5] Ryo Karakida, Shotaro Akaho, and Shun-ichi Amari. Universal statistics of Fisher information in deep neural networks: Mean field approach. In *Proceedings of International Conference on Artificial Intelligence and Statistics (AISTATS)*; (*arXiv1806.01316*), pages 1032–1041, 2019.
- [6] Arthur Jacot, Franck Gabriel, and Clément Hongler. Neural tangent kernel: Convergence and generalization in neural networks. In *Advances in neural information processing systems (NeurIPS)*, pages 8571–8580, 2018.
- [7] Shun-ichi Amari. *Information geometry and its applications*. Springer, 2016.
- [8] Ryo Karakida, Shotaro Akaho, and Shun-ichi Amari. The normalization method for alleviating pathological sharpness in wide neural networks. In *Advances in neural information processing systems (NeurIPS)*, 2019.
- [9] Yann LeCun, Ido Kanter, and Sara A. Solla. Eigenvalues of covariance matrices: Application to neural-network learning. *Physical Review Letters*, 66(18):2396–2399, 1991. ISSN 00319007. doi: 10.1103/PhysRevLett.66.2396.
- [10] Andrew M Saxe, James L McClelland, and Surya Ganguli. Exact solutions to the nonlinear dynamics of learning in deep linear neural networks. *ICLR 2014*, *arXiv:1312.6120*, 2014.
- [11] Jeffrey Pennington, Samuel Schoenholz, and Surya Ganguli. The emergence of spectral universality in deep networks. In *Proceedings of International Conference on Artificial Intelligence and Statistics (AISTATS)*, pages 1924–1932, 2018.
- [12] Lechao Xiao, Yasaman Bahri, Jascha Sohl-Dickstein, Samuel S Schoenholz, and Jeffrey Pennington. Dynamical isometry and a mean field theory of CNNs: How to train 10,000-layer vanilla convolutional neural networks. In *Proceedings of International Conference on Machine Learning (ICML)*, pages 5393–5402, 2018.
- [13] Piotr A Sokol and Il Memming Park. Information geometry of orthogonal initializations and training. *ICLR 2020*, *arXiv:1810.03785*, 2020.
- [14] Dan V Voiculescu. Symmetries of some reduced free product C^* -algebras. In *Operator Algebras and their Connections with Topology and Ergodic Theory*, volume 1132 of *Lecture Notes in Math.*, pages 556–588. Springer, Berlin, 1985.

- [15] Dan V Voiculescu. Limit laws for random matrices and free products. *Invention Math.*, 104: 201–220, 1991.
- [16] Razvan Pascanu and Yoshua Bengio. Revisiting natural gradient for deep networks. *ICLR 2014*, *arXiv:1301.3584*, 2014.
- [17] Frederik Kunstner, Lukas Balles, and Philipp Hennig. Limitations of the empirical Fisher approximation. In *Advances in neural information processing systems*, 2019.
- [18] Dan V Voiculescu. Multiplication of certain non-commuting random variables. *J. Operator Theory*, 18:223–235, 1987.
- [19] Jeffrey Pennington, Samuel Schoenholz, and Surya Ganguli. Resurrecting the sigmoid in deep learning through dynamical isometry: theory and practice. In *Advances in neural information processing systems (NeurIPS)*, pages 4785–4795, 2017.
- [20] Dan V Voiculescu, Ken J Dykema, and Alexandru Nica. *Free random variables*. Number 1 in CRM Monograph Series. American Mathematical Soc., 1992.
- [21] James A Mingo and Roland Speicher. *Free probability and random matrices*, volume 35 of *Fields Institute Monograph*. Springer-Verlag New York, 2017.
- [22] Boris Hanin and Mihai Nica. Products of many large random matrices and gradients in deep neural networks. *Communications in Mathematical Physics*, 376:1–36, 2019.
- [23] Greg Yang. Scaling limits of wide neural networks with weight sharing: Gaussian process behavior, gradient independence, and neural tangent kernel derivation. *arXiv:1902.04760*, 2019.
- [24] Leonid Pastur. On random matrices arising in deep neural networks: Gaussian case. arXiv preprint, *arXiv:2001.06188*, 2020.
- [25] Serban Teodor Belinschi. The atoms of the free multiplicative convolution of two probability distributions. *Integral Equations and Operator Theory*, 46(4):377–386, 2003.
- [26] Han Xiao, Kashif Rasul, and Roland Vollgraf. Fashion-MNIST: a novel image dataset for benchmarking machine learning algorithms. arXiv preprint, *arXiv:1708.07747*, 2017.
- [27] Wei Hu, Lechao Xiao, and Jeffrey Pennington. Provable benefit of orthogonal initialization in optimizing deep linear networks. *ICLR 2020*, *arXiv:2001.05992*, 2020.
- [28] Fumio Hiai and Dénes Petz. Asymptotic freeness almost everywhere for random matrices. *Acta scientiarum mathematicarum*, 66(3-4):809–834, 2000. ISSN 0001-6969.

A Proof for The Two-Hidden-Layer Case

Here we provide the postponed proof.

Proof. Set $\tilde{\nu}_\ell = (\gamma_\ell^{-1} \cdot)_* \nu_\ell = \alpha_\ell \delta_1 + (1 - \alpha_\ell) \delta_0$. Then we have

$$\mu_3 = (q_2 + \sigma_3^2 \gamma_2 \cdot)_* [\tilde{\nu}_2 \boxtimes (q_1 + \sigma_2^2 \gamma_1 q_0 \cdot)_* \tilde{\nu}_1]. \quad (\text{A.1})$$

By replacing $\sigma_{\ell+1}^2 \gamma_\ell q_{\ell-1} q_\ell^{-1}$ with γ_ℓ ($\ell = 1, 2$), we may assume that $q_\ell = \sigma_\ell = 1$. Write

$$\xi = (1 + \gamma_1 \cdot)_* \tilde{\nu}_1. \quad (\text{A.2})$$

Since $S_{\tilde{\nu}_2 \boxtimes \xi}(z) = S_{\tilde{\nu}_2}(z) S_\xi(z)$, we have $h_\xi^{-1}(z) = h_{\tilde{\nu}_2 \boxtimes \xi}^{-1}(z) S_{\tilde{\nu}_2}(z)$. Hence $h_{\tilde{\nu}_2 \boxtimes \xi}(z)$ is the solution of the following equation on w :

$$w = h_\xi(z S_{\tilde{\nu}_2}(w)). \quad (\text{A.3})$$

Note that

$$S_{\tilde{\nu}_2}(z) = \frac{z+1}{z+\alpha_2}, \quad (\text{A.4})$$

$$h_\xi(z) = z \left[\frac{1-\alpha_1}{z-1} + \frac{\alpha_1}{z-1-\gamma_1} \right] - 1. \quad (\text{A.5})$$

Thus the solution of (A.3) is given by

$$w = \frac{g(z) \pm z \sqrt{-f(z)}}{2(z-1)(1+\gamma_1-z)}, \quad (\text{A.6})$$

where

$$f(z) = (\lambda_+ - z)(z - \lambda_-), \quad (\text{A.7})$$

$$\lambda_\pm = 1 + \gamma_1 \left(\sqrt{\alpha_1(1-\alpha_2)} \pm \sqrt{\alpha_2(1-\alpha_1)} \right)^2, \quad (\text{A.8})$$

$$g(z) = (z-1)(z-2(1+\gamma_1)\alpha_2) - \gamma_1(\alpha_1 - \alpha_2)z. \quad (\text{A.9})$$

By $G(z) = (h(z) + 1)/z$ and by the condition $\Im G(z) < 0$ if $\Im z > 0$, we have

$$G_{\tilde{\nu}_2 \boxtimes \xi}(z) = \frac{1}{z} \left[1 + \frac{g(z)}{2(z-1)(1+\gamma_1-z)} \right] + \frac{\sqrt{-f(z)}}{2(z-1)(1+\gamma_1-z)}. \quad (\text{A.10})$$

Note that $1 \leq \lambda_- \leq \lambda_+ \leq 1 + \gamma_1$. By Stieltjes inversion formula, the absolutely continuous part of $\nu \boxtimes \mu$ is given by

$$-\frac{1}{\pi} \lim_{y \rightarrow +0} \Im G_{\tilde{\nu}_2 \boxtimes \xi}(x + y\sqrt{-1}) = \frac{\sqrt{f(x)}}{2\pi(x-1)(1+\gamma_1-x)} \mathbf{1}_{\{f \leq 0\}}(x) \quad (x \in \mathbb{R}). \quad (\text{A.11})$$

Weights of the atoms are given by

$$\lim_{y \rightarrow +0} z G_{\tilde{\nu}_2 \boxtimes \xi}(y\sqrt{-1}) = 1 - \alpha_2, \quad (\text{A.12})$$

$$\lim_{y \rightarrow +0} (z-1) G_{\tilde{\nu}_2 \boxtimes \xi}(1 + y\sqrt{-1}) = (\alpha_2 - \alpha_1)^+, \quad (\text{A.13})$$

$$\lim_{y \rightarrow +0} (z-1-\gamma_1) G_{\tilde{\nu}_2 \boxtimes \xi}(1 + \gamma_1 + y\sqrt{-1}) = (\alpha_1 + \alpha_2 - 1)^+, \quad (\text{A.14})$$

where $a^+ = \max(a, 0)$ for $a \in \mathbb{R}$. By [25], the free multiplicative convolution $\tilde{\nu}_2 \boxtimes \xi$ has no singular continuous part. Hence $\tilde{\nu}_2 \boxtimes \xi$ is the sum of the absolutely continuous part (A.11) and the pure point part (A.12, A.13, A.14) as follows:

$$(\tilde{\nu}_2 \boxtimes \xi)(dx) = (1 - \alpha_2) \delta_0(dx) + (\alpha_2 - \alpha_1)^+ \delta_1(dx) + (\alpha_1 + \alpha_2 - 1)^+ \delta_{1+\gamma_1}(dx) \quad (\text{A.15})$$

$$+ \frac{\sqrt{(\lambda_+ - x)(x - \lambda_-)}}{2\pi(x-1)(1+\gamma_1-x)} \mathbf{1}_{[\lambda_-, \lambda_+]}(x)(dx). \quad (\text{A.16})$$

It holds that $\mu_3 = (1 + \gamma_2 \cdot)_*(\tilde{\nu}_2 \boxtimes \xi)$. We have completed the proof. \square

B Out of Initial Spectral Distribution

We show how different the pointwise FIM H_L 's spectral distribution during training was from that in the initial state. We focus on areas near the boundary $\eta = 2/L$ at large L . Recall that the test loss reduced, but the test accuracy did not improve in the boundary areas with $\eta > 2/L$. Fig. 5 shows that eigenvalue distributions of H_L near the boundary at large L . We observed that most of the eigenvalue distributions shrunk in the areas with $\eta > 2/L$. The shrinkage in the eigenvalue distribution is the reason for the reduction in test loss in the areas.

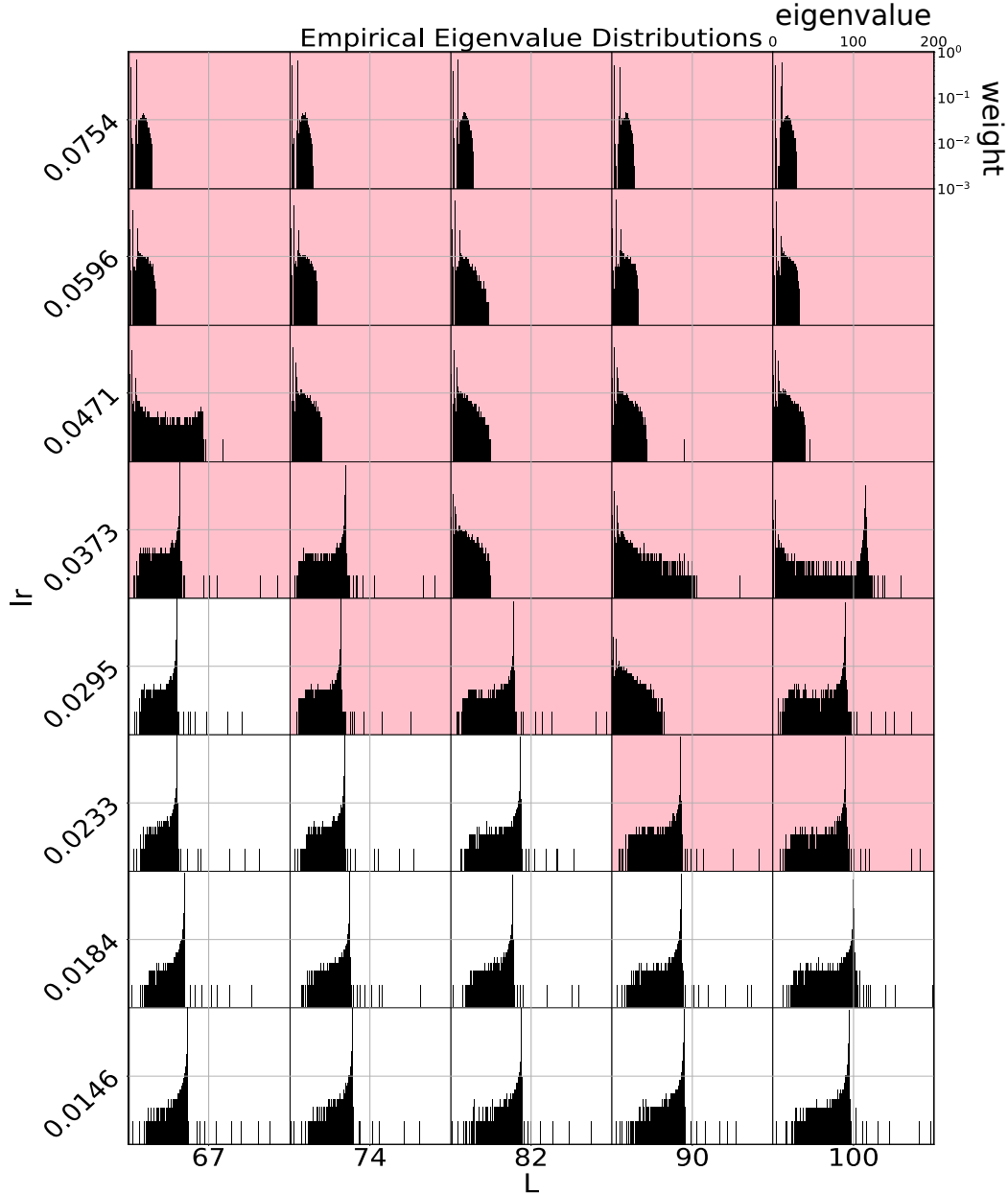


Figure 5: Histograms of eigenvalue distributions after training 500-steps. All histograms share the x-axis (eigenvalue) and the y-axis (weight). The y-axis is logarithmic. The outer frame's x-axis represents the depth L and its y-axis represents the learning rate η . Both axes are logarithmic. The histograms in the red region belong to $\eta > 2/L$, and the others belong to $\eta \leq 2/L$.

C A Short Introduction to Asymptotic Freeness for Machine Learning

C.1 Comparison with Classical Probability Theory

Asymptotic freeness is the vital notion in free probability theory. In order to introduce asymptotic freeness to readers in the machine learning community, we explain the freeness by comparing free probability theory to classical probability theory. We refer readers to [21] or [20] for the detail.

| | r.v. | moments | for multiple r.v.s | independence |
|-----------|------|-------------------|--------------------|-------------------------------------|
| classical | X | $\mathbb{E}[X^k]$ | joint distribution | decomposition of joint distribution |
| free | A | $\text{tr}[A^k]$ | joint moments | decomposition of joint moments |

Table 1: Comparison of free and classical probability theory.

Firstly, consider a matrix $A \in M_M(\mathbb{C})$. We denote by A^* the complex conjugate of A . Assume that A is self-adjoint, that is, $A^* = A$. Then the spectral distribution, denoted by μ_A , is given by

$$\mu_A = \frac{1}{N} \sum_{\lambda \in \sigma(A)} \delta_\lambda, \quad (\text{C.1})$$

where $\sigma(A) = \{\lambda \in \mathbb{C} \mid A - \lambda I \text{ is invertible}\} \subset \mathbb{R}$, and I is the identity operator. We emphasize that the spectral distribution is determined by its moments. That is, a distribution μ is equal to μ_A if and only if

$$\text{tr}(A^k) = \int x^k \mu(dx) \quad (k \in \mathbb{N}), \quad (\text{C.2})$$

where tr is the normalized trace so that $\text{tr}(I) = 1$. In other words, the family of moments $\text{tr}(A^k)$ ($k \in \mathbb{N}$) has the same information as the spectral distribution μ_A . Now consider a counterpart of the spectral distribution at classical probability theory. Let X be a real random variable and μ_X be the distribution of X . If μ_X is compactly supported, the distribution μ_X is determined by the moments:

$$\mathbb{E}[X^k] = \int x^k \mu_X(dx) \quad (k \in \mathbb{N}). \quad (\text{C.3})$$

By comparing (C.2) and (C.3), we see that the self-adjoint operator A corresponds to a real random variable and the spectral distribution μ_A corresponds to the distribution of the random variable.

Secondly, consider multiple matrices. Let $A_1, A_2 \in M_M(\mathbb{C})$ be non-commuting self-adjoint matrices. As an example, consider the distribution of the sum of them. The spectral distribution of the sum $A_1 + A_2$ is determined by its moments

$$\text{tr}[(A_1 + A_2)^k] = \sum_{i_1, i_2, \dots, i_k \in \{1, 2\}} \text{tr}[A_{i_1} A_{i_2} \cdots A_{i_k}] \quad (k \in \mathbb{N}). \quad (\text{C.4})$$

Hence the trace of all words on A_1 and A_2 determines the spectral distribution $\mu_{A_1 + A_2}$. Now consider its counterpart at classical probability theory. Let X_1 and X_2 be real random variables. Then

$$\mathbb{E}[(X_1 + X_2)^k] = \sum_{m=1}^k \binom{k}{m} \text{tr}[X_1^m X_2^{k-m}] \quad (k \in \mathbb{N}). \quad (\text{C.5})$$

By comparing (C.4) and (C.5), we need much more information to determine the distribution for non-commuting matrices than for commuting real random variables. Therefore, we extend the definition of the joint distribution in a different way from that in the classical probability theory. For a family of matrices $(A_j)_{j \in J}$, its *joint moments* are trace of all words in the family, which are given by

$$\text{tr}[A_{j_1} A_{j_2} \cdots A_{j_k}] \quad (j_1, j_2, \dots, j_k \in J, k \in \mathbb{N}). \quad (\text{C.6})$$

Note that we use the joint moments as a counterpart of the joint distribution, which is a probability distribution in classical probability theory and does not exist for non-commuting matrices.

Lastly, consider the notion of independence. The independence in the classical probability theory means that the joint distribution of multiple random variables decomposed to the product of marginal distributions of each random variable. Since we consider the joint moments for multiple operators, we extend the concept of independence as a decomposition law of joint moments to each operator's moments. The freeness is one of the decomposition laws of joint moments (see Table 1).

C.2 Freeness

Summarizing above, we formulate the free algebra, the tracial state, and introduce the freeness.

Let us denote by $\mathbb{C}\langle Z_j \mid j \in J \rangle$ the free \mathbb{C} -algebra of indeterminates $(Z_j)_{j \in J}$, which is the algebra of polynomials of noncommutative variables given by the weighted sum of words as follows:

$$\mathbb{C}\langle Z_j \mid j \in J \rangle = \{ \alpha_\emptyset 1 + \sum_{k=1}^{\infty} \sum_{j_1, \dots, j_k \in J} \alpha_{j_1, j_2, \dots, j_k} Z_{j_1} Z_{j_2} \dots Z_{j_k}, \quad (\text{C.7})$$

$$\text{where } \alpha_* \in \mathbb{C} \text{ is zero except for finite number of indices } \}. \quad (\text{C.8})$$

We introduce an adjoint operation $*$ on $\mathbb{C}\langle Z_j \mid j \in J \rangle$ (using universality) by

$$(\alpha_{j_1, j_2, \dots, j_k} Z_{j_1} Z_{j_2} \dots Z_{j_k})^* = \overline{\alpha_{j_1, j_2, \dots, j_k}} Z_{j_k} \dots Z_{j_2} Z_{j_1}. \quad (\text{C.9})$$

Next, we introduce the tracial state, which is an abstracted notion of the normalized trace of matrices and the expectation operator to random variables.

Definition C.1. A *tracial state* τ on $\mathcal{A} = \mathbb{C}\langle Z_j \mid j \in J \rangle$ is a \mathbb{C} -valued map satisfying the following conditions.

1. $\tau(1) = 1$.
2. $\tau(\alpha a + \beta b) = \alpha \tau(a) + \beta \tau(b)$ ($a, b \in \mathcal{A}, \alpha, \beta \in \mathbb{C}$).
3. $\tau(a^*) = \overline{\tau(a)}$ ($a \in \mathcal{A}$).
4. $\tau(ab) = \tau(ba)$ ($a, b \in \mathcal{A}$).

The first condition is the normalization so that the total volume becomes 1. The fourth one is the tracial condition.

Here we have prepared to introduce the freeness.

Definition C.2. Given two families $a = (a_j)_{j \in I}$ and $b = (b_j)_{j \in J}$ in \mathcal{A} are said to be *free* (or *free independent*) with respect to τ if the following decomposition of joint moments follows: For any $k \in \mathbb{N}$, any $p_1, p_2, \dots, p_k \in \mathbb{C}\langle X_i \mid i \in I \rangle$, and any $q_1, q_2, \dots, q_k \in \mathbb{C}\langle Y_j \mid j \in J \rangle$, it holds that

$$\tau[p_1(a)q_1(b)p_2(a)q_2(b) \dots p_k(a)q_k(b)] = 0 \quad (\text{C.10})$$

if $\tau[p_m(a)] = \tau[q_m(b)] = 0$ ($m = 1, 2, \dots, k$).

Example C.3. Assume that Z_1 and Z_2 are free. Write $Z_j^\circ = Z_j - \tau(Z_j)$. Then

$$\text{Cov}(Z_1, Z_2) = \tau(Z_1 Z_2) - \tau(Z_1)\tau(Z_2) = \tau(Z_1^\circ Z_2^\circ) + \tau(Z_1^\circ)\tau(Z_2) + \tau(Z_1)\tau(Z_2^\circ) = 0. \quad (\text{C.11})$$

Here we use the freeness to eliminate the first term. From this equation, we see that free variables are uncorrelated. The difference between freeness and classical independence appears in the decomposition of higher moments such as $\tau(Z_1 Z_2 Z_1 Z_2)$.

C.3 Infinite Dimensional Approximation of Random Matrices

Here we introduce the relation between freeness and random matrices.

Definition C.4. Let $A_i(M), B_j(M) \in M_M(\mathbb{C})$ ($M \in \mathbb{N}, i \in I, j \in J$). Then the families $(A_i)_{i \in I}$ and $(B_j)_{j \in J}$ are said to be *asymptotically free* as $M \rightarrow \infty$ if there exists \mathcal{A}, τ , and $a_i \in \mathcal{A}$ ($i \in I$) and $b_j \in \mathcal{A}$ ($j \in J$) so that

$$\lim_{M \rightarrow \infty} \text{tr}(A_i(M)^k) = \tau(a_i^k) \quad (k \in \mathbb{N}, i \in I), \quad (\text{C.12})$$

$$\lim_{M \rightarrow \infty} \text{tr}(B_j(M)^k) = \tau(b_j^k) \quad (k \in \mathbb{N}, j \in J), \quad (\text{C.13})$$

$$\text{and, } (a_i)_{i \in I} \text{ and } (b_j)_{j \in J} \text{ are free.} \quad (\text{C.14})$$

Here we introduce a known result in free probability theory.

Proposition C.5 ([28, Prop. 3.5]). *For each $M \in \mathbb{N}$, consider the following matrices. Let $U(M)$ be random matrix uniformly distributed on $M \times M$ unitary matrices (resp. orthogonal matrices). Let $A(M)$ and $B(M)$ be complex (resp. real) self-adjoint random matrices independent of $U(M)$. Assume that there exist two compactly supported distributions μ and ν such that the following limits hold almost surely.*

$$\lim_{M \rightarrow \infty} \text{tr}[A(M)^k] = \int x^k \mu(dx) \quad (k \in \mathbb{N}), \quad (\text{C.15})$$

$$\lim_{M \rightarrow \infty} \text{tr}[B(M)^k] = \int x^k \nu(dx) \quad (k \in \mathbb{N}). \quad (\text{C.16})$$

Under the above conditions, it holds that $B(M)$ and $U(M)^ A(M) U(M)$ are asymptotically free as $M \rightarrow \infty$ almost surely. Furthermore, when $A(M)$ and $B(M)$ are positive definite, then the limit distribution of $B(M)^{1/2} U(M)^* A(M) U(M) B(M)^{1/2}$ is the multiplicative free convolution $\mu \boxtimes \nu$.*

Note that random matrices $A(M)$ and $B(M)$ do not have to be independent in Proposition C.5.

C.4 Application to the FIM

Let H_ℓ be the pointwise FIM and $A_\ell := W_\ell H_\ell W_\ell^*$. Then H_ℓ and A_ℓ are independent because A_ℓ does not contain the component W_ℓ . Recall that we assume that D_ℓ and (W_ℓ, W_ℓ^*) are asymptotic free, and W_ℓ is uniformly distributed on orthogonal matrices. By the above conditions, it holds that $W_\ell^* A_\ell W_\ell$ and D_ℓ^2 are asymptotic free as the wide limit $M \rightarrow \infty$ by Proposition C.5. Then the limit spectral distribution of $D_\ell H_\ell D_\ell = D_\ell W_\ell^* A_\ell W_\ell D_\ell$ is equal to $\mu_\ell \boxtimes \nu_\ell$, where μ_ℓ (resp. ν_ℓ) is the limit spectral distribution of H_ℓ (resp. D_ℓ^2).